

# A Semi-Analytical Model for Two Phase Immiscible Flow in Porous Media Honouring Capillary Pressure

F. Hussain · Y. Cinar · P. Bedrikovetsky

Received: 15 November 2010 / Accepted: 11 October 2011 / Published online: 3 November 2011  
© Springer Science+Business Media B.V. 2011

**Abstract** This article describes a semi-analytical model for two-phase immiscible flow in porous media. The model incorporates the effect of capillary pressure gradient on fluid displacement. It also includes a correction to the capillarity-free Buckley–Leverett saturation profile for the stabilized-zone around the displacement front and the end-effects near the core outlet. The model is valid for both drainage and imbibition oil–water displacements in porous media with different wettability conditions. A stepwise procedure is presented to derive relative permeabilities from coreflood displacements using the proposed semi-analytical model. The procedure can be utilized for both before and after breakthrough data and hence is capable to generate a continuous relative permeability curve unlike other analytical/semi-analytical approaches. The model predictions are compared with numerical simulations and laboratory experiments. The comparison shows that the model predictions for drainage process agree well with the numerical simulations for different capillary numbers, whereas there is mismatch between the relative permeability derived using the Johnson–Bossler–Naumann (JBN) method and the simulations. The coreflood experiments carried out on a Berea sandstone core suggest that the proposed model works better than the JBN method for a drainage process in strongly wet rocks. Both methods give similar results for imbibition processes.

**Keywords** Two phase flow · Porous medium · Semi-analytical model · Coreflood · Relative permeability

## List of Symbols

$D$  Velocity of the shock front  
 $f$  Fractional flow of water phase

---

F. Hussain · Y. Cinar (✉)  
University of New South Wales, Sydney, NSW 2052, Australia  
e-mail: y.cinar@unsw.edu.au

P. Bedrikovetsky  
University of Adelaide, Adelaide, SA 5005, Australia

$f'_s$	Derivative of fractional flow w.r.t. saturation
$F_{w\_wet}$	Fraction of the water-wet rock surface
$J$	Leverett function
$k$	Permeability
$k_{ro}$	Oil relative permeability
$k_{ro\_max}$	Maximum oil relative permeability
$k_{rw}$	Water relative permeability
$k_{rw\_max}$	Maximum water relative permeability
$L$	Core length
$n$	Exponent for Corey-type power law
$p$	Pressure
$P_c$	Capillary pressure
$s$	Water phase saturation
$s_i$	Initial water saturation
$s_{ir}$	Irreducible water saturation
$s^0$	Maximum water saturation, equals to unity minus residual/critical oil saturation
$t$	Time
$T$	Dimensionless time, p.v. injection
$T_p$	Pore volumes produced
$T_{op}$	Pore volumes of oil produced
$T_{wp}$	Pore volumes of water produced
$U$	Velocity
$x$	Linear coordinate, from injectors towards producers
$X$	Dimensionless linear coordinate
$\lambda$	Total mobility of the oil-water fluid
$\Psi$	Potential for capillary forces
$\varepsilon$	Capillary-viscous ratios
$\xi$	Self-sharpening large scale (slow) coordinate
$\omega$	Travelling wave fast coordinate near to the displacement front
$\zeta$	Fast coordinate near to the core outlet
$\phi$	Porosity
$\mu$	Fluid viscosity
$\sigma$	Interfacial tension
$\theta$	Contact angle

### Subscripts and Superscripts

W, O	Water, oil
i	Initial (of water saturation)
0	Boundary value on the injector (saturation, flux)
BL	Buckley–Leverett
BT	Breakthrough
SZ	Stabilized zone
ee	End effect
min	Minimum

## 1 Introduction

Reservoir engineering calculations require input data regarding rock and fluid properties. Among these, relative permeability is one of the most important and critical properties which control recovery of fluids from reservoirs. Relative permeability can be measured through steady-state and unsteady-state laboratory experiments. Steady-state experiments allow direct measurement of relative permeability although they are time consuming compared to unsteady-state experiments. Moreover, flow conditions in steady-state experiments do not depict reservoir flow mechanisms which include displacement of one fluid by another. It was reported that unsteady-state methods had been used more frequently (Christiansen 2001).

A detailed discussion about different analytical/semi-analytical methods for predicting relative permeabilities from unsteady state tests has been presented by Hussain et al. (2010). It is known that neglecting capillary pressure in deriving relative permeabilities from experiments leads to erroneous results (Kalbus and Christiansen 1995; Nordtvedt et al. 1999; Qadeer et al. 2002; Bedrikovetsky 1993). Yet, most of the analytical methods do not include the effects of capillary pressure (Jones and Roszelle 1978; Welge 1952; Johnson et al. 1959; Toth et al. 2002). Instead, high injection rate/pressure gradient is used to minimize these effects, which is significantly higher than the pressure gradients seen at the reservoir scale (Honarpour et al. 1986). Qadeer (2001) and Alizadeh et al. (2007) reported experimental data showing that the application of high rates may not result in the desired control of capillary end effects. Another limitation of analytical methods is that they generate very limited data scanning only post-breakthrough fluid saturations.

Civan and Donaldson (1989) and Udegbumam (1991) described semi-analytical approaches for relative permeability determination. Moreover, Hussain et al. (2010) proposed a modification in the semi-analytical approach described by Civan and Donaldson (1989). Like analytical methods, these methods also generate data only for fluid saturations after breakthrough. However, the semi-analytical approaches include capillary pressure in the modified-Darcy equation used in the pressure drop calculations. For this reason, these methods are thought to generate more reliable data compared to analytical methods. However, they still use the capillarity-free Buckley–Leverett solution to generate saturation profiles in the core (Welge 1952). These models are therefore unable to properly model the capillary discontinuity at the outlet of the core known as capillary end effects.

Odeh and Dotson (1985) and Kalbus and Christiansen (1995) proposed corrections for capillary end effects on the results derived using the JBN method (Johnson et al. 1959). These corrections are valid only for drainage tests. Kalbus and Christiansen (1995) found that the correction proposed by Odeh and Dotson (1985) did not produce reliable results for their experimental data. Similar observations have recently been made by Hussain et al. (2010) for the correction proposed by Kalbus and Christiansen (1995). Islam and Bentsen (1986) proposed that experimental measurements of saturation and pressure distribution along the length of the core should be made in order to account for capillary end effects. Such experiments, however, require quite sophisticated experimental setups. Huang and Honarpour (1998) presented an analytical approach for correcting capillary end effects on the JBN results. They derived the flow model for  $T = \infty$ , which corresponds to end point relative permeability only.

Another approach to determine relative permeabilities from displacement experiments is history matching, which includes finding a solution of the inverse problem by minimizing the difference between the measured data and the predictions of a numerical model (Poulsen et al. 2000; Qadeer 2001; Tsakiroglou et al. 2004; Subbey et al. 2006; Basbug and Karpyn 2008; Krause et al. 2011). Two advantages of history matching over analytical models are

that capillary pressure is directly included in the flow equations and that data for the whole saturation interval can be obtained. Qadeer (2001) defined zero capillary pressure at the inlet and outlet ends of a rock sample to model capillary end effects. He observed that, at low injection rates, it is difficult to obtain a good match between experimental and simulated data. He used X-ray CT imaging to observe capillary end effects and stabilized zone along the core during flooding experiments and used the observed saturation distributions to match the simulated saturation distribution. Recently, Perrin and Benson (2010) reported high-rate displacement experiments in which they did not observe any capillary end effects. As a result, they did not include these effects in their history matching.

History matching is an inverse problem and hence the resultant match is not unique and also depends on the choice of the functional representation of relative permeability (Tikhonov et al. 1977; Subbey et al. 2006). Therefore, this approach may give stable results only for fixed analytical expressions of relative permeability (Batycky et al. 1981; Richmond et al. 1990; Qadeer et al. 1988; Chardaire-Riviere et al. 1992; Sigmund and McCaffery 1979). Nevertheless, very different shapes of relative permeability have been reported in the literature (Honarpour et al. 1986; Kerig and Watson 1986), which reduces the stability of the optimization method. Some researchers used spline functions and found that more complicated shapes of relative permeabilities can be generated using these functions (Kerig and Watson 1986; Hussain et al. 2010; Subbey et al. 2006). Hussain et al. (2010) demonstrated that the non-uniqueness problem can be tackled to some extent using spline functions.

One way for the solution of the inverse problem is the use of a semi-analytical solution for the direct problem. Bedrikovetsky et al. (1996) proposed a method for matching the capillary-pressure-free Buckley–Leverett solution with the local asymptotic solutions around the shock front (stabilized zone solution) and in the neighbourhood of the core outlet after breakthrough (end effect solution). Their model produces data for water flooding in a water-wet core. One of the advantages of their model is that it can generate relative permeabilities for the whole fluid saturations.

In this article, we extend the work of Bedrikovetsky et al. (1996) for different types of fluid injection and wettability conditions. First, saturation profiles are generated before and after breakthrough by matching the capillary-free Buckley–Leverett solution with the stabilized zone solution and the end effect solution, respectively. Afterwards, the modified-Darcy equation is used to calculate the pressure drop across the core using the generated saturation profiles. We present a stepwise procedure for generating the saturation profiles and calculating the pressure drop.

## 2 Two-Phase Displacement with Capillary Pressure

Two-phase displacement of immiscible incompressible liquids (i.e. oil and water) in porous media is described by the mass balance equation for water and modified-Darcy's law for two phases accounting for capillary pressure (Rapoport and Leas 1953; Barenblatt et al. 1991)

$$\frac{\partial s}{\partial T} + \frac{\partial f(s)}{\partial X} = \varepsilon \frac{\partial^2 \Psi(s)}{\partial X^2} \quad (1)$$

$$\varepsilon = \sigma \cos \theta \sqrt{k\Phi} / \mu_o UL \quad (2)$$

$$f(s) = (1 + k_{ro} \mu_w / k_{rw} \mu_o)^{-1} \quad (3)$$

$$\Psi'_s(s) = -k_{ro}(s) f(s) J'_s(s) \quad (4)$$

$$1 = -\frac{k\lambda(s)}{LU} \frac{\partial P_W}{\partial X} - \varepsilon k_{ro}(s) \frac{\partial J(s)}{\partial X} \tag{5a}$$

$$1 = -\frac{k\lambda(s)}{LU} \frac{\partial P_o}{\partial X} + \varepsilon \frac{\mu_o}{\mu_w} k_{rw}(s) \frac{\partial J(s)}{\partial X} \tag{5b}$$

where  $s$  is the saturation of water phase,  $f(s)$  is the fractional flow function that is equal to the fraction of water in the overall flux under zero capillary pressure and  $J(s)$  is the dimensionless capillary pressure (Leverett’s function). Equation 1 is the volume balance equation for incompressible water phase; water is transported by the advective flux proportional to fractional flow, and by the capillary flux (expression in the right hand side). Equation 5 is the modified-Darcy’s equation for the total two-phase flux and shows two components of two-phase flow, i.e. the advective and capillary fluxes. Equations 1 and 5 determine two unknowns, i.e. saturation  $s(X, T)$  and pressure  $P(X, T)$ . Either of Eqs. 5a or 5b to determine pressures in water ( $P_W$ ) or in oil ( $P_o$ ) can be used.

Dimensionless parameter  $\varepsilon$  (Eq. 2) is the capillary-viscous number which represents the ratio between the average capillary pressure and the pressure drop across the core at the beginning of the displacement. From Eq. 2 one can see that, for very long cores,  $\varepsilon$  is small, so the terms of its order can be neglected. In this article,  $\varepsilon$  is considered to be a small parameter.

The solution of Eqs. 1–5 is defined by one initial condition and two boundary conditions.

### 2.1 Initial Condition

The initial condition for Eq. 1 describes the initial saturation profiles in the core. For water injection, the experiment is started at irreducible water saturation:

$$T = 0: s = s_i = s_{ir} \tag{6}$$

For oil injection, the experiment is started with the core fully saturated with water:

$$T = 0: s = s_i = 1 \tag{7}$$

### 2.2 Inlet Boundary Condition

For water injection, the boundary condition at the inlet of the core corresponds to the single-phase water flow:

$$X = 0: f - \varepsilon \frac{\partial \Psi(s)}{\partial X} = 1 \tag{8}$$

For oil injection, water influx at the inlet is zero:

$$X = 0: f - \varepsilon \frac{\partial \Psi(s)}{\partial X} = 0 \tag{9}$$

Similar to the initial condition, the inlet boundary condition only depends on the type of fluid injection and not on the wettability preference of the core.

### 2.3 Outlet Boundary Condition

Before breakthrough, the fluid saturation at the outlet boundary is equal to the initial fluid saturation. Hence, the fractional flow of the displacing phase is zero. Once the displacing phase reaches the outlet boundary, the flow mechanism is affected by the capillary discontinuity at the outlet. At the outlet, there is a fluid distribution head, whose permeability is

much higher than the core and hence the capillary pressure in it is close to zero (Barenblatt et al. 1991; Donnez 2007). For the system to remain at capillary equilibrium, the capillary pressure at the core outlet must be the same as in the fluid distribution head. For this reason, the saturation of the wetting phase at the outlet must reach its maximum to meet the capillary pressure condition in the fluid distribution head.

In an imbibition process (the displacing phase is wetting), as soon as the displacing phase reaches the outlet, it spreads across the outlet to reach zero capillary pressure which corresponds to a maximum saturation of the wetting phase. Until this to happen, there is no production of the displacing phase. When this happens, then the wetting phase production starts. On the contrary, in a drainage process (the displacing phase is non-wetting), the saturation of the wetting phase is already at its maximum. As soon as the displacing phase reaches the outlet, the production of the displacing phase starts while the wetting phase remains at its maximum.

The discussion above suggests that the outlet boundary condition should be defined before and after breakthrough separately. Before breakthrough, the outlet saturation condition corresponds to the initial conditions (Eqs. 6 and 7) hence the out-flux of the water phase is constant. After breakthrough, the wetting phase saturation should correspond to zero capillary pressure. Note that, before breakthrough, the outlet boundary condition depends on initial fluid saturations whereas, after breakthrough, on the core wettability only.

For water injection into a water-wet core (imbibition), before breakthrough ( $T < T_{BT}$ ), the outlet water saturation has its irreducible value,  $s_{ir}$  (Eq. 6), i.e. the flux of water is zero at the outlet. After breakthrough ( $T > T_{BT}$ ), water reaches its maximum saturation (the residual oil saturation) to meet the zero capillary pressure condition. This is formulated as it follows:

$$X = 1: \begin{cases} f - \varepsilon \frac{\partial \Psi(s)}{\partial X} = 0 & T < T_{BT} \\ s = s^0 & T \geq T_{BT} \end{cases} \tag{10}$$

For oil injection into a water-wet core (drainage), before breakthrough, the outlet water saturation is unity which corresponds to the 100% water flux. After breakthrough, water retains its maximum saturation, representing the zero capillary pressure. Note that the after breakthrough condition is the same as Eq. 10 because of the same wettability condition. The mathematical formulation of this boundary is given by:

$$X = 1: \begin{cases} f - \varepsilon \frac{\partial \Psi(s)}{\partial X} = 1 & T < T_{BT} \\ s = s^0 & T \geq T_{BT} \end{cases} \tag{11}$$

For water injection into an oil-wet core (drainage), the before breakthrough condition is the same as Eq. 10 because of the same initial condition (the outlet water saturation is irreducible,  $s_{ir}$ ). After breakthrough, the water saturation remains at its minimum ( $s_{ir}$ ) because the wetting phase (oil) has to attain its maximum saturation for the zero capillary pressure condition. This is given by

$$X = 1: \begin{cases} f - \varepsilon \frac{\partial \Psi(s)}{\partial X} = 0 & T < T_{BT} \\ s = s_{ir} & T \geq T_{BT} \end{cases} \tag{12}$$

For oil injection into an oil-wet core (imbibition), the before breakthrough condition is the same as Eq. 11 because of the same initial condition whereas the after breakthrough condition is the same as (12) because of the same wettability condition. Hence

$$X = 1: \begin{cases} f - \varepsilon \frac{\partial \Psi(s)}{\partial X} = 1 & T < T_{BT} \\ s = s_{ir} & T \geq T_{BT} \end{cases} \tag{13}$$

In the above equations, before breakthrough, the saturation distribution at the outlet depends on the type of the fluid injected or initial fluid saturations and not on the wettability of the core. However, after breakthrough, it depends on the wettability of the core and not on the type of the fluid injected. The wetting phase saturation reaches its maximum at the outlet because of the capillary end effects.

Equations 10–13 can be used for both weak and strong wettability conditions. Equation 2 defines the capillary number which accounts for the wettability ( $\cos \theta$ ). For a neutrally wet rock (i.e.  $60 < \theta < 120^\circ$ ),  $\varepsilon$  becomes zero which reduces the solution of Eqs. 1–5 to the Buckley–Leverett solution which will be described in Sect. 3. There is another classification of wettability in literature known as the fractionally wet (Anderson 1987) which represents a medium composed of oil- and water-wet sections. Anderson (1987) discussed a special type of fractionally wet rocks, namely mixed-wet in which the oil-wet surfaces form a continuous path. They further reported that mixed wettability has been observed in reservoir rocks such as carbonates that have microporosity. It is therefore worthwhile to discuss the boundary conditions for the mixed-wet systems as well.

For a core having ‘ $F_{W\_wet}$ ’ fraction of the pores strongly water-wet, we can rewrite the above outlet boundary conditions. Before breakthrough, boundary conditions remain unchanged because they are independent of wettability. After breakthrough, the water-wet surfaces retain a maximum water saturation ( $s^0$ ) and oil-wet surfaces retain a maximum oil saturation ( $s_{ir}$ ). The boundary condition for water injection into a mixed-wet core then becomes,

$$X = 1: \left\{ \begin{array}{ll} f - \varepsilon \frac{\partial \Psi(s)}{\partial X} = 0 & T < T_{BT} \\ s = F_{W\_wet} s^0 + (1 - F_{W\_wet}) s_{ir} & T \geq T_{BT} \end{array} \right\} \tag{14}$$

while the boundary for oil injection into a mixed-wet core is given by,

$$X = 1: \left\{ \begin{array}{ll} f - \varepsilon \frac{\partial \Psi(s)}{\partial X} = 1 & T < T_{BT} \\ s = F_{W\_wet} s^0 + (1 - F_{W\_wet}) s_{ir} & T \geq T_{BT} \end{array} \right\} \tag{15}$$

The Rapoport–Leas equation (Eq. 5) is a non-linear parabolic equation; it requires a boundary condition at the core outlet ( $X = 1$ ). The effluent boundary condition depends on wettability and the state of the medium on the right to the core, i.e. at  $X = 1 + 0$ . Barenblatt et al. (1991) proposed to consider a free space to the right of the core as a porous medium with infinite permeability, where the capillary pressure tends to zero. The condition of continuity of the phase pressures requires the capillary pressure to be continuous as well. So, the capillary pressure at  $X = 1 + 0$  must be zero. For water-wet media, it implies that  $s = 1 - s_{or}$ . It means that water completely fills the outlet cross section and displaces oil from there up to its residual value.

In Sect. 3, we solve the 1-D coreflood problem that honours the capillary pressure by the method of *matched asymptotic expansions*.

### 3 Large Scale Approximation: Buckley–Leverett Equation

Barenblatt et al. (1991) described the applicability of the Buckley–Leverett solution using the large scale approximation. If the length scales of the porous medium are of the order of distance between wells, i.e. hundreds of meters, the pressure difference is of the order of tens or units of MPa and flow velocity is of the order  $10^{-6}$  to  $10^{-5}$  m/s. Capillary pressure for the rocks with permeabilities of the order  $0.1 - 1.0 \mu\text{m}^2$  ranges  $10^{-4}$  to  $10^{-2}$  MPa, respectively.

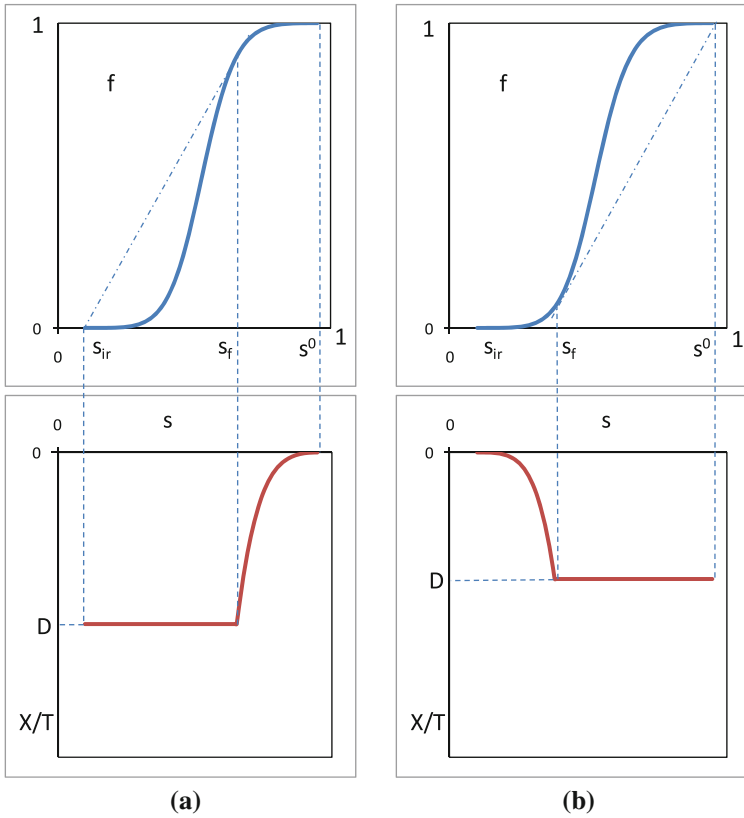


**Fig. 1** Graphical solution of 1-D Buckley–Leverett problem: (a) water injection (b) oil injection

Consequently, viscous forces are much higher as compared to capillary forces and the capillary number,  $\epsilon$  becomes small ( $10^{-2}$  to  $10^{-4}$ ). For small  $\epsilon$ , one can neglect the right hand side of Eq. 1 to obtain the Buckley–Leverett equation (Buckley and Leverett 1942):

$$\frac{\partial s}{\partial T} + \frac{\partial f(s)}{\partial X} = 0 \tag{16}$$

where the function  $f(s)$  represents the fractional flow and is the ratio between the water flux and the total flux. The shape of  $f(s)$  is shown in Fig. 1. Tending  $\epsilon$  to zero corresponds to an equality of phase pressures  $P_w$  and  $P_o$ . Note that, for smaller scales such as laboratory flow tests, the value of capillary pressure may be significant as compared to the total pressure drop across the rock. This limits the use of Eq. 16 for the laboratory flow test analysis.

Since Eq. 16 is of the first order, just one boundary condition is required. This can be the injected flux which can be regulated during the injection; therefore the boundary condition at the inlet is used. As  $\epsilon$  approaches 0, Eqs. 8 and 9 become:

$$X = 0: f = 1 \tag{17}$$

for water injection and

$$X = 0: f = 0 \tag{18}$$

for oil injection. The solution  $s(X,T)$  of the 1-D capillary-pressure-free displacement problem (Eqs. 16–18) is self-similar, depending only on the parameter  $\xi = X/T$ . The Riemann solution of hyperbolic Eq. 16 consists of the rarefaction water and shock front (Barenblatt et al. 1991; Bedrikovetsky 1993). For water injection,

$$\xi = f'_s(s); \quad 0 < \xi < D; \quad D = f(s_f)/(s_f - s_i) = f'_s(s_f) \tag{19}$$

$$s = s_{ir}; \quad D < \xi < \infty \tag{20}$$

and for oil injection

$$\xi = f'_s(s); \quad 0 < \xi < D; \quad D = f(s_f)/(s_f - s_{ir}) = f'_s(s_f) \tag{21}$$

$$s = 1; \quad D < \xi < \infty \tag{22}$$

The frontal saturation corresponds to the tangent point between the  $f$ – $f$  curve and the straight line drawn from the initial saturation point, the slope of this line is equal to the displacement front velocity  $D$ .

The geometric interpretation of the continuous solutions given in Eqs. 19–22 is the saturation value  $s$ , which corresponds to the value of self-similar coordinate and is equal to the slope of  $f$ – $f$  curve at point  $s$  (Fig. 1). This allows for a graphical analytical construction of the saturation profile as shown in Fig. 1.

The solution given in Eqs. 19–22 is valid for any wettability preference and is the outer asymptotic expansion (Kevorkian et al. 1981; Van Dyke 1975; Nayfeh 1973) for the displacement problem that honours the capillary pressure.

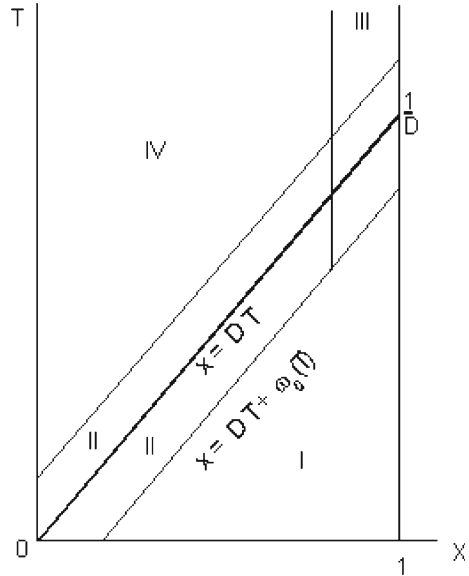
### 4 Matching the Asymptotic Expansions

The right hand side in Eq. 1 can be neglected when the saturation gradient is of an order of unity with  $\varepsilon$  going to zero. This is the case in zones I and IV shown in Fig. 2 where the solution is continuous and the gradient is limited. In the neighbourhood of the shock front ( $X = DT$ ), a continuous change of saturation takes place from the initial to the frontal one. The size of this zone of continuous change in the saturation is  $\varepsilon$  and known as the stabilized zone (zone II in Fig. 2). Asymptotic solution of Eq. 1 with  $\varepsilon > 0$  in zone II has to match two values of saturation in the solution of Eq. 16 in the large scale approximation: the initial and frontal saturations.

There also appears a zone of the sharp variation of saturation in the neighbourhood of the core outlet. The reason for this is the disappearance of the boundary conditions (Eqs. 10–15) in the capillarity-free Buckley–Leverett solution (Eqs. 19–22). Therefore, the boundary condition (Eqs. 10–15) determines the saturation at the outlet boundary after the breakthrough for every small value of  $\varepsilon$ . Nevertheless, for the case where  $\varepsilon = 0$ , the saturation at the outlet is determined by the solution given in Eqs. 19 and 21. The size of the zone of the continuous change is  $\varepsilon$  as well.

Zone III of the continuous sharp change of saturation near the core outlet is shown in Fig. 2. The asymptotic solution of Eq. 1 with  $\varepsilon$  tending to zero in zone III matches the solution given in Eqs. 19 and 21 with the saturation at the core outlet given by the boundary condition (Eqs. 10–15).

**Fig. 2** Capillary pressure boundary layers with matching asymptotic expansions



### 5 Stabilized Zone in the Neighbourhood of the Displacement Front

In this section, we discuss the saturation distribution in the neighbourhood of the displacement front  $X = DT$  (Barenblatt et al. 1991; Gel'fand 1959). Let us introduce a travelling wave coordinate in the reference system linked with the displacement front as below:

$$\omega = \frac{X - DT}{\epsilon} \tag{23}$$

For the conventional linear coordinate  $X$ , the value of the core length is unity and the size of the stabilized zone is of an order of  $\epsilon$ . The new coordinate is equal to zero on the trajectory of the displacement front. The scaling of  $\omega$  in  $1/\epsilon$  times expands the stabilized zone to the size of unity and shifts the boundaries of the reservoir to the plus and minus infinity as  $\epsilon$  tends to zero.

The stabilized zone is basically the transition zone where the saturation distribution has the form of a travelling wave (Fig. 3). The detailed physics of the stabilized zone has been described by Rapoport and Leas (1953) and Barenblatt et al. (1991). The Buckley–Leverett solution neglects capillary pressure which results in a shock front, with an abrupt change of saturation from  $S_i$  to  $S_f$  at the front. However, in reality capillary pressure causes physical dispersion which creates a transition zone (stabilized zone) instead of a shock front. The width of the stabilized zone is determined as the distance between the points where the saturations differ from the limiting values  $S_i$  and  $S_f$ . Bacri et al. (1985) experimentally showed that the width of the stabilized zone increases with time. As the stabilized zone propagates, the breakthrough recovery decreases.

The average displacing phase saturation in the stabilized zone is less than the shock front saturation  $S_f$  (Fig. 3). As a result, the breakthrough recovery becomes less compared to the Buckley–Leverett solution. For this reason, the stabilized zone can play a significant role in immiscible fluid displacement before breakthrough and therefore must be incorporated in the flow model.

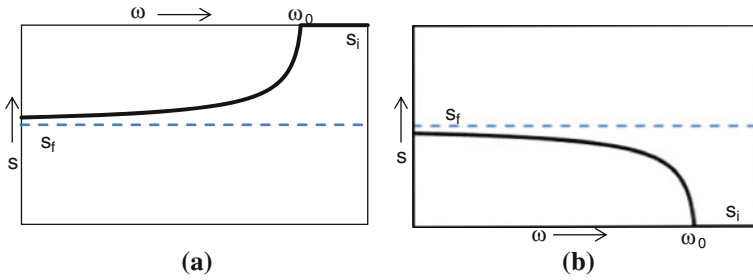


**Fig. 3** Profile of saturation distribution in the stabilized zone; (a) water injection and (b) oil injection

Appendix A shows that neglecting the term of the order of  $\epsilon$  in the governing Eq. A-3 in this reference system results in a steady-state solution (A-7). The solution is given by Eqs. A-10 and A-11 for the co-ordinates  $(X, T)$ . The plot of the solution is given in Fig. 3.

The saturation decreases continuously in the stabilized zone from the frontal value  $s_f$  on the minus infinity to the initial one  $s_i$  when  $\omega = \omega_0$ . For  $\omega$  approaching  $\omega_0$  the saturation is equal to  $s_i$ . Solution of Eqs. A-10 and A-11 is not unique because of the unknown term  $\omega_0$ . It can be calculated using material balance which is discussed in Appendix B.

### 6 Global Asymptotic Solution Before the Breakthrough

For matching the asymptotic solution in the stabilized zone Eqs. A-10 and A-11 with the outer solution (Eqs. 19–22), we use the method proposed by Erdélyi (1956). Introduce a shock-function which is the shock on the displacement front in the Buckley–Leverett solution (Eqs. 19–22):

$$s_{sh}(X, T) = \begin{cases} s_i, & \text{if } X > DT \\ s_f, & \text{if } X < DT \end{cases} \tag{24}$$

The formula for the continuous solution is given by:

$$s(X, T) = s_{BL}(X/T) + s_{sz}(X - DT/\epsilon, T) - s_{sh}(X - DT) \tag{25}$$

Here the first term is the outer (Buckley–Leverett) solution given by Eqs. 19–22, the second term is the stabilized zone solution (Eqs. A-10 and A-11) and the third term is the shock wave (Eq. 24). It can be noted that, in the neighbourhood of the shock front (zone II in Fig. 2), the Buckley–Leverett solution approaches to the shock function. Hence, the first and third terms of Eq. 25 cancel each other and the saturation becomes equal to  $s_{sz}$ . Otherwise  $s_{sz} \approx s_{sh}$  and the saturations in the core are equal to the Buckley–Leverett saturations. The plot of the solution given by Eq. 25 is shown in Fig. 4 (curve 2).

The proposed solution (Eq. 25) contains a free parameter which is the function  $\omega_0(T)$ . This function can be found from the condition of material balance at each moment  $T$ . In Appendix B, the expression for the global asymptotic solution (Eq. 25) is substituted in the material balance equation (Eq. B-1), which is obtained from the continuity equation (Eq. 1). The final expressions (Eqs. B-5 and B-6 or B-12 and B-13) are the equations which determine the function  $\omega_0(T)$  for each moment  $T$ . Equations 15, A-8, B-5 and B-6 present the solution of the 1-D coreflood problem that honours the capillary pressure before breakthrough.

The saturation profiles are shown in Fig. 4 before the breakthrough for the Buckley–Leverett solution (curve 1) and for the global asymptotic solution (curve 2). In the vicinity

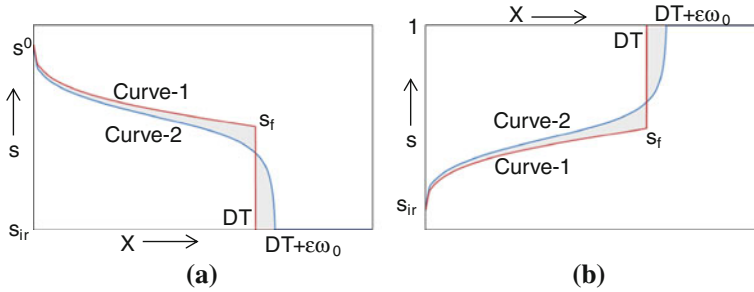


**Fig. 4** Buckley Leverett (curve-1) and global asymptotic solution (curve-2) profiles of saturation distribution before breakthrough; (a) water injection and (b) oil injection

of the displacement front, the saturation changes gradually due to the capillary pressure, so the asymptotic solution smoothens the shock in the Buckley–Leverett solution. The asymptotic solution exhibits the constant velocity of the saturation wave propagation, where the trajectory of the saturation front (this is not a shock front but a weak discontinuity) is given by

$$X = DT + \epsilon\omega_0 (T) \tag{26}$$

The condition of the material balance (Eqs. B-1 and B-8), which allows us to determine the position of the stabilized zone (Eqs. B-6 and B-13), means that the two shaded areas shown in Fig. 4 are equal.

### 7 Solution for the End-Effect Zone

In this section, we discuss the solution of Eq. 1 in the neighbourhood of the core outlet  $X = 1$  (Barenblatt et al. 1991). Let us introduce the inner coordinate

$$\zeta = (1 - X)/\epsilon \tag{27}$$

In Appendix C, it is shown that neglecting the term of an order of  $\epsilon$  in the governing equation (Eq. C-1) in this reference system results in a steady-state solution given by Eqs. C-7, C-8 and C-9. Further, we call Eqs. C-7, C-8 and C-9 the ‘end effect solution’. The plot of the solution is shown in Fig. 5.

### 8 Global Asymptotic Solution After the Breakthrough

The method of the matched asymptotic expansions (Erdélyi 1956) results in the continuous solution after breakthrough:

$$s(X, T) = s_{BL}(X/T) + s_{ee}((1 - X)/\epsilon, T) - s_{BL}(1/T) \tag{28}$$

The saturation profile in Eq. 28 is shown in Fig. 6. The third term in Eq. 28 is the limit of the second term. The term  $(s_{BL}(1/T))$  can be calculated from Eqs. 19 and 21 for  $X = 1$ . In the region away from the core outlet, the difference between the second and the third terms tends to zero and Eq. 28 becomes the Buckley–Leverett solution (Eqs. 19 and 21). In the same way, the first term tends to the third term when approaching to the core outlet, so the

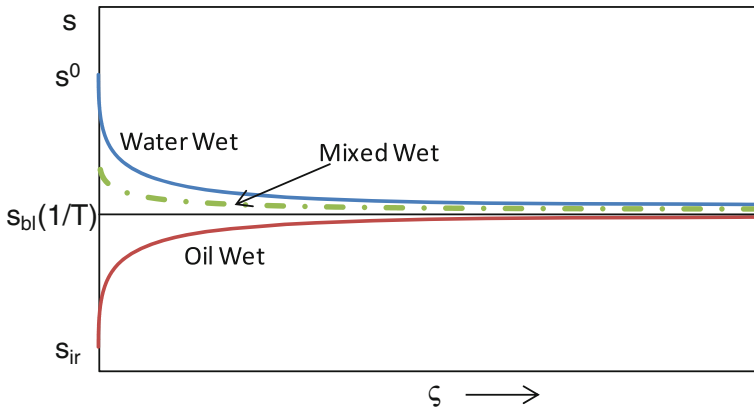


**Fig. 5** Distribution of saturation in the end-effect zone

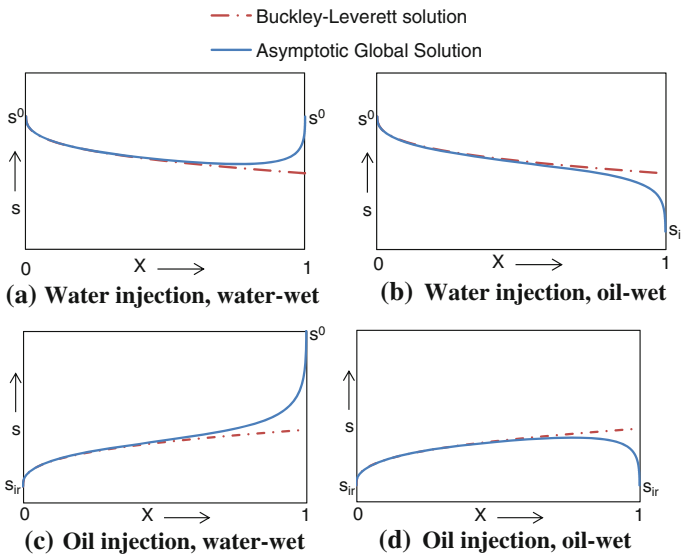


**Fig. 6** Buckley-Leverett and global asymptotic solution profiles of saturation distribution after breakthrough

difference between the first and the third terms tends to zero around the outlet. Therefore, in the neighbourhood of the outlet, Eq. 28 becomes the end-effect solution (Eqs. C-7, C-8 and C-9).

### 9 Solution Procedure

In this section, we describe a semi-analytical procedure which requires an initial guess of relative permeabilities. The JBN derived relative permeabilities may be used for this purpose. In order to update relative permeabilities during the iterative process, relative permeabilities are defined by parametric mathematical functions. Corey-type power law or a cubic spline

function can be used for this purpose (Hussain et al. 2010). For the data analysis of the experiments discussed in Sect. 10.2, we used Corey-type power law:

$$k_{rw} = k_{rw\_max} \left( \frac{s - s_{ir}}{s^0 - s_{ir}} \right)^{n_w} \tag{29}$$

$$k_{ro} = k_{ro\_max} \left( 1 - \frac{s - s_{ir}}{s^0 - s_{ir}} \right)^{n_o} \tag{30}$$

Moreover, the model requires the prior information about experimental injection rates, fluid and core properties, i.e. fluid viscosities, core dimensions, porosity, permeability, wettability and capillary pressure. Amongst these properties the measurement of capillary pressure is quite complicated. The capillary pressure can be measured using different methods (Amyx et al. 1960). If these measurements are not available, rock permeability can be used to derive capillary pressure data. A number of researchers have described the relationship between capillary pressure and permeability based on the fact that both properties depend upon pore size distribution of the rock (Purcell 1949; Burdine et al. 1950). Purcell (1949) presented the following equation:

$$k = \frac{(\sigma \cos \theta)^2}{2} \phi \sum_{j=1}^n \frac{s_j}{(P_c)_j^2} \tag{31}$$

Detailed derivation of the above equation is given in Amyx et al. (1960).

The steps for determining relative permeability from the coreflood data using the described model are given below:

- Step 1: Calculate the  $f - f$  curve using the available estimate of relative permeabilities. Calculate the frontal saturation ( $s_f$ ) and frontal velocity ( $D$ ); as shown in Fig. 1.
- Step 2: At a particular moment  $T$ , calculate the Buckley–Leverett saturation profile ( $s_{bl}$  vs.  $X$ ) using Eqs. 19–22.
- Step 3: If  $T$  (in step 2)  $< T_{BT}$ 
  - a. Calculate  $\omega_0$  using Eq. B-7 or B-14.
  - b. Calculate  $s(-DT/\varepsilon)$  using Eqs. B-6 or B-13.
  - c. Calculate the stabilized zone saturation profile ( $s_{sz}$  vs.  $X$ ) using Eq. A-10 or A-11.
  - d. Determine the saturation profile in the core using Eq. 25.
- If  $T$  (in step 2)  $\geq T_{BT}$ 
  - a. Use Eq. C-7, C-8 or C-9 to determine the end-effect saturation profile ( $s_{ee}$  vs.  $X$ ).
  - b. Determine the saturation profile in the core using Eq. 28.
- Step 4: Using the saturation profile from step-3, calculate pore volumes of displaced fluid production using the following equations
  - a. For water injection

$$T_{op} = \int_0^1 s(X, T) dX - s_{ir} \tag{32}$$

b. For oil injection

$$T_{wp} = 1 - \int_0^1 s(X, T) dX \quad (33)$$

Step 5: Using the saturation profile from step-3, calculate the pressure drop in the core using Eq. D-3 or D-4.

Step 6: Repeat steps (2–5) for different moments  $T$ .

Step 7: Plot pore volumes produced (calculated in step-4) and pressure drop (calculated in step-5) versus  $T$ .

Step 8: Compare the results in step-7 with the measured pressure and production data. If the mismatch is acceptable, the initial guess of the relative permeabilities is correct. Otherwise update the relative permeabilities and repeat steps-1 through -8 until an acceptable match is obtained between the predictions and experimental observations. In order to update relative permeabilities, the parameters of the selected mathematical function defining relative permeabilities are changed (for example  $s_{ir}$ ,  $s^0$ ,  $k_{ro\_max}$ ,  $k_{rw\_max}$ ,  $n_w$  and  $n_o$  in Eqs. 29 and 30) in the following way:

- The value of  $s_{ir}$  is set to the minimum wetting-phase saturation obtained from the porous plate capillary pressure test (Kalbus and Christiansen 1995; Hussain et al. 2010).
- For an imbibition experiment, the experimentally determined end-point saturation is used for  $s^0$  for the matching purpose. For drainage experiments,  $s^0$  is taken unity.
- As a result, the number of the matching parameters is reduced to four, namely  $k_{ro\_max}$ ,  $k_{rw\_max}$ ,  $n_w$  and  $n_o$ .
- To update the relative permeability values after the first iteration, the matching parameters are changed by 10% and the second iteration is run. For the third iteration the percent change in the matching parameters is proportional to the difference in the results of the first and second iterations. This process continues until a match is obtained.

It can be observed that the proposed procedure requires determining various integrals. For this, any appropriate numerical algorithm can be used (Hamming 1986).

## 10 Validation and Results

The validation of the proposed model was carried out by comparing the model predictions with numerical simulations as well as experiments conducted on a Berea sandstone core.

### 10.1 Numerical Simulation

We ran finite-difference numerical simulations with assumed relative permeabilities to produce production and pressure drop data for different values of capillary number,  $\epsilon$ . This simulated production and pressure drop data was then used to calculate relative permeabilities using the procedure described above. Use of numerical simulation instead of experimental data has the advantage that true relative permeabilities (input relative permeabilities in simulations) are already known which can be compared with the model predictions. We also used the simulated data to produce JBN results.

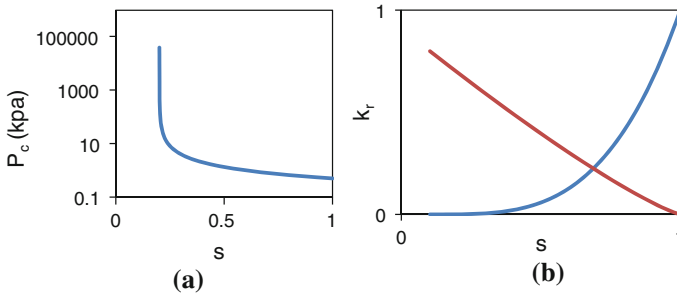
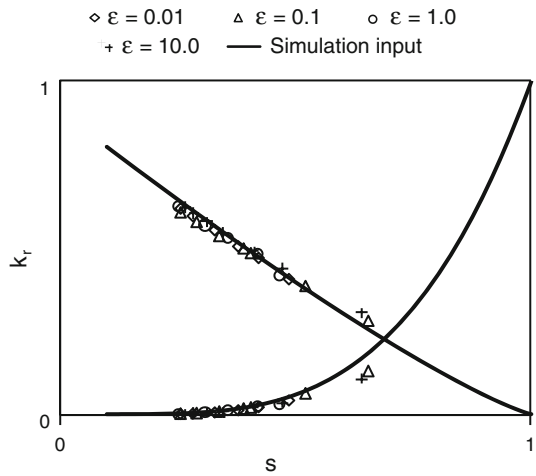


**Fig. 7** Input data for simulations (a) capillary pressure and (b) relative permeabilities

**Fig. 8** Comparison of JBN predicted relative permeabilities with input relative permeabilities in simulations



Oil flooding in a strongly water-wet core was studied ( $\cos \theta = 1$ ) for four different capillary numbers ( $\varepsilon = 0.01, 0.1, 1.0$  and  $10.0$ ). Figure 7 shows the input capillary pressure and relative permeability data. Figure 8 compares the JBN predicted relative permeabilities and true relative permeabilities.

We followed the semi-analytical procedure described in Sect. 9. It was found that, for low to moderately high values of capillary numbers ( $\varepsilon = 0.01, 0.1$  and  $1$ ), the model produces an optimum match with the simulated production and pressure drop data for true relative permeabilities. While for  $\varepsilon = 10.0$  the match is poor. The quality of match is shown in Fig. 9. From these results we can conclude that the proposed model gives reliable predictions for the following condition

$$\varepsilon < 1.0 \quad \text{or} \quad \sigma \cos \theta \sqrt{k\Phi} / \mu_o UL \leq 1 \tag{34}$$

This condition should be used to design the displacement tests. There are a few parameters to vary in order to achieve the required capillary number. Usually the injection rate is increased to decrease the capillary number. But, very high injection rates may not be suitable because this restricts to record enough data points to capture important features of the relative permeability curves. Also, it is possible with high rates to deviate from the laminar flow which is a prerequisite for applying Darcy’s law. Assuming that one pore volume per minute injection

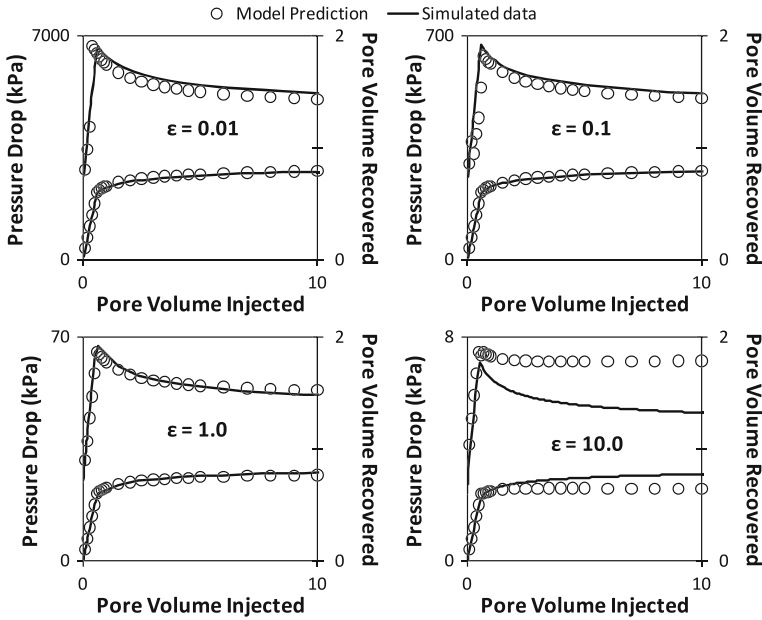


Fig. 9 Comparison of model predictions and simulated data—match quality

can furnish enough data points for the analysis; Eq. 34 can be used to derive a minimum length of the core in the experiments

$$L_{\min}^2 = \frac{60\sigma \cos \theta}{\mu_o} \sqrt{\frac{k}{\phi}} \tag{35}$$

or for strong wetting conditions ( $\cos \theta = 1$ )

$$L_{\min}^2 = \frac{60\sigma}{\mu_o} \sqrt{\frac{k}{\phi}} \tag{36}$$

For a data set of rock permeability ( $k$ ) = 250 mD, porosity ( $\phi$ ) = 0.2, oil viscosity ( $\mu_o$ ) = 0.0015 Pa s and interfacial tension ( $\sigma$ ) = 0.038 N/m, we obtain an estimate for the minimum core length of 4 cm.

From the production data (Fig. 9), it can be observed that the wetting phase recovery decreases as the capillary number increases. Fig. 10 shows the wetting phase recovery at different capillary numbers. The reason for this is that, at higher capillary numbers, a large amount of the wetting phase is trapped at the core outlet due to capillary end effects, resulting in a lower recovery.

### 10.2 Experiments

A drainage and an imbibition test were conducted on a strongly water-wet Berea sandstone core. Table 1 summarizes the properties of the rock and fluids used. Experimental production and pressure drop data are shown in Fig. 11. The core was first saturated with 2% NaCl brine (the wetting phase). The temperature was kept at 25°C in an oven while the outlet pressure

**Fig. 10** Wetting phase recovery as a function of capillary number

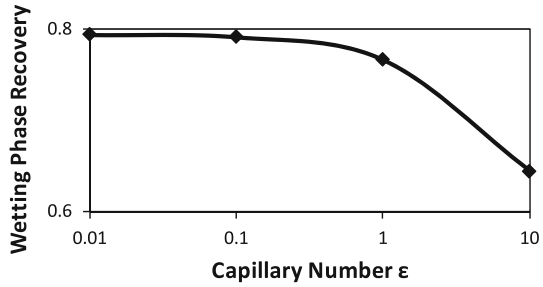


**Table 1** Rock and fluid properties

	$L$ (cm)	$L_{min}$ (cm)	$\phi$	$k$ (mD)	Fluids	$\rho$ (g/cc)	$\mu$ (cP)	$\sigma$ (mN/m)
Berea	7.8	3.72	0.21	200	Brine	1.007	0.95	38
					Soltrol	0.748	1.46	

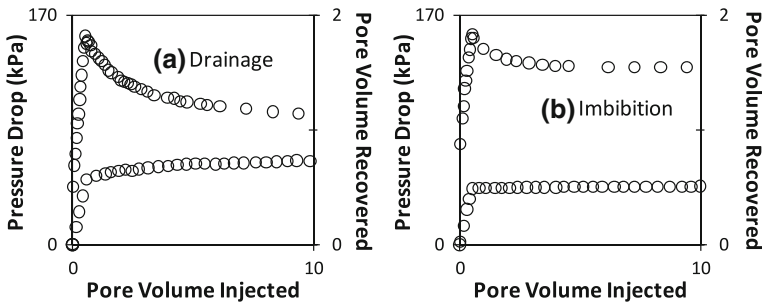


**Fig. 11** Experimental pressure drop and production data

was open to the atmosphere for both tests. A constant injection rate of 5 cc/min was maintained during both drainage and imbibition cycles, which corresponds to a capillary number ( $\epsilon$ ) of 0.45. Figure 12 shows the comparison of the model predicted drainage and imbibition relative permeabilities with the JBN results.

### 11 Discussion

The proposed model accounts for capillary pressure effects in coreflood experiments. The global asymptotic solution ( Fig. 6) shows that, for imbibition experiments, the wetting phase saturation reaches its maximum as  $T \rightarrow \infty$ . Thus, the ultimate recovery from an imbibition displacement is independent of the capillary number. On the contrary, for drainage experiments, there is always a finite volume of the wetting phase trapped at the outlet due to capillary end effects. Hence, in drainage displacements, the wetting phase saturation is higher than its irreducible saturation. Therefore, the ultimate recovery from a drainage displacement depends on the capillary number. This observation can be deduced from the model results (Fig. 10). Similar observations have been made from the experimental data reported (Hussain et al. 2010; Kalbus and Christiansen 1995).

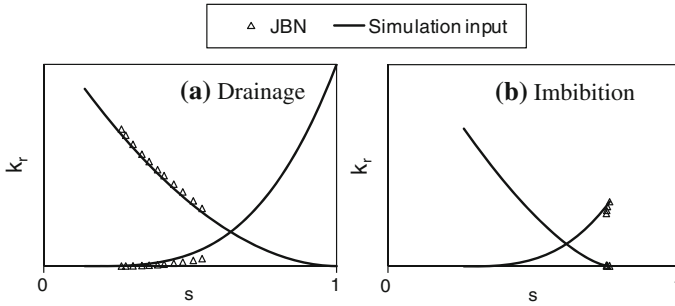


**Fig. 12** Comparison of model predictions and JBN results

It was expected that the JBN relative permeabilities strongly depend on the injection rate. But Fig. 8 does not show this effect. It may be due to the fact that numerical simulations used in this study do not model capillary end-effects.

Figure 12 shows a significant difference for the end-point values between the proposed model and the JBN results, although this difference is negligible for the imbibitions process. This is because Berea sandstone is strongly water-wet. For a drainage process in a strong water-wet rock, the residual water saturation is high because of the capillary end effects. The post-breakthrough data corresponds to low wetting phase saturations where capillary pressure is higher. On the other hand, for an imbibition process in a strong water-wet rock, the frontal saturation ( $s_f$ ) is very close to the maximum water saturation ( $s^0$ ). That is why capillary end effects are insignificant. There is also not much oil production after the breakthrough because of the high recovery at the breakthrough.

From numerical simulations and coreflood experiments, we can conclude that, for strong wetting conditions, capillary end effects control the drainage process and as a result the JBN predictions are erroneous. However, for the imbibitions process, the JBN predictions agree well with the proposed model because of negligible capillary end effects. In the cases where weak wetting conditions prevail, capillary end effects become significant in imbibition processes as well and the proposed model offers better estimates for relative permeability.

## 12 Conclusions

Matching the asymptotic expansions around the shock wave and upstream the core outlet with the large scale hyperbolic Riemann solution and its application to determining the relative phase permeabilities from laboratory coreflooding allows drawing the following conclusions:

- A semi-analytical model has been proposed which accounts for capillary pressure gradient in the flow equations. The proposed model involves the corrections for the stabilized zone in the neighbourhood of the displacement front and for the end effects at the outlet. The proposed model is applicable for a wide range of capillary pressures, displacement rates and core lengths at different wettability conditions.
- Numerical simulations and experimental results have validated the proposed model predictions.
- The proposed model generates reliable estimates of relative permeabilities for a capillary number equal to or less than unity ( $\epsilon \leq 1$ ). From this condition, a generic criterion has been derived to calculate the minimum core length required to obtain reliable experimental data

for determining relative permeability. This data is then used to capture important features of relative permeability curves.

- Under strong wetting conditions, capillary end effects have strong effect on drainage displacements, whereas it is insignificant in an imbibition process.

**Acknowledgments** The first author acknowledges UET Lahore of Pakistan for sponsoring his PhD studies at UNSW. The authors acknowledge the research grants provided by the Australian Research Council under contracts DP0878564 and DP1094299. We also thank Sefer Yanici for providing the capillary pressure data.

### Appendix A: Asymptotic Solution for the Stabilized Zone

Following Buckley and Leverett (1942) and Rapoport and Leas (1953), we derive the saturation distribution in the stabilized zone in the neighbourhood of the front  $X = DT$ . Equation 1 can be transformed into a new coordinate system as defined by Eq. 23:

$$\varepsilon \frac{\partial s}{\partial T} + \frac{\partial f}{\partial \omega} - D \frac{\partial s}{\partial \omega} = \frac{\partial^2 \Psi}{\partial \omega^2} \tag{A-1}$$

Neglecting the  $\varepsilon$ -order term on the left hand side of Eq. A-1, we obtain an ordinary differential equation. Now, this second order equation can be reduced to a first order equation:

$$\frac{d\Psi}{d\omega} = f - Ds + \text{const.} \tag{A-2}$$

Analyzing Eq. 23 shows that the new coordinate ( $\omega$ ) is equal to zero on the trajectory of the displacement front.

$$\omega \rightarrow 0: \quad X = DT \tag{A-3}$$

Moreover, if  $\omega$  approaches + infinity or -infinity,  $\varepsilon$  tends to zero and the solution of Eq. 1 approaches the capillarity-free Buckley–Leverett solution. Hence, for any point  $(X, T)$ , if the point is located ahead of the front, the  $s(X, T)$  tends to approach the initial water saturation; if the point is located behind the front, the  $s(X, T)$  tends to approach the frontal water saturation.

$$\omega \rightarrow \infty: \quad s = s_i \tag{A-4}$$

$$\omega \rightarrow -\infty: \quad s = s_f \tag{A-5}$$

The boundary condition given by Eq. A-4 allows us to determine the constant on the right hand side of Eq. A-2, separately for water and oil injections. For water injection ( $s_i = s_{ir}$ )

$$\frac{d\Psi}{d\omega} = f - D(s - s_{ir}) \tag{A-6}$$

and for oil injection ( $s_i = I$ )

$$\frac{d\Psi}{d\omega} = D(1 - s) - (1 - f) \tag{A-7}$$

Equation A-6 can be integrated from an initial saturation ( $s_i$ ) to any saturation ( $s$ ). For water injection

$$\int_{s_{ir}}^s \frac{\Psi'(s) ds}{f - D(s - s_{ir})} = \omega - \omega_0 \tag{A-8}$$

and for oil injection

$$\int_1^s \frac{\Psi'(s) ds}{D(1-s) - (1-f)} = \omega - \omega_0 \tag{A-9}$$

Let us analyze the solution given by Eqs. A-8 and A-9 as  $s$  approaches  $s_i$ . Assuming that near to the saturation  $s_i$  the  $f$ - $f$  function is of an order of  $(s - s_i)^\beta$ , and  $\beta > 1$ , which is the usual case (Honarpour et al. 1986; Barenblatt et al. 1991) and the Buckley–Leverett function is of an order of  $(s - s_i)^\alpha$ , and  $\alpha > 0$ , which is the requirement for the finiteness of the capillary pressure. We find that the integral on the left hand side of Eqs. A-8 and A-9 converges. Assigning the value  $s(\omega_0) = s_i$ , for the positive values of  $\omega - \omega_0$ , we obtain  $s=s_i$  and, for the negative values of  $\omega - \omega_0$ , the solution of the problem is given by Eqs. A-8 and A-9.

Now let us analyze the solution (Eqs. A-8 and A-9) as  $s$  approaches  $s_f$ . With the same assumptions about the fractional flow and the capillary pressure curves, we obtain that the denominator of the integrant of Eqs. A-10 and A-11 is of an order of  $(s - s_f)^2$ . The numerator remains limited, so the integral diverges. As a result, the independent variable  $\omega$  tends to the negative infinity. The solution satisfies Eqs. A-1, A-4 and A-5 for any constant  $\omega_0$ . The solution takes the form given by Eqs. A-8 and A-9. For water injection

$$\int_{s_{ir}}^s \frac{\Psi'(s) ds}{f - D(s - s_{ir})} = \frac{X - DT}{\varepsilon} - \omega_0(T) \tag{A-10}$$

and for oil injection

$$\int_1^s \frac{\Psi'(s) ds}{D(1-s) - (1-f)} = \frac{X - DT}{\varepsilon} - \omega_0(T) \tag{A-11}$$

So the solution given by Eqs. A-10 and A-11 is steady-state solution in the reference system linked with the displacement front. Therefore, it is called as the ‘stabilized zone solution’.

### Appendix B: Matching the Stabilized Zone Solution with the Buckley–Leverett Solution

Erdélyi (1956) proposed the following method of matching the discontinuous outer solution with the stabilized zone solution. The continuous solution is described by Eq. 25. Let us find the free-parameter  $\omega_0$  from the condition of the material balance. The integral of Eq. 27 w.r.t.  $X$  ( $0 \rightarrow 1$ ) should be equal to the volume of water currently present in the core. For water injection

$$\int_0^1 (s_{BL} + s_{SZ} - s_{sh})dX - s_{ir} = T \tag{B-1}$$

Because the capillarity-free Buckley Leveret solution also conserves the material balance:

$$\int_0^1 s_{BL}(X, T)dX - s_{ir} = T \tag{B-2}$$

Comparing Eqs. B-1 and B-2, we obtain the condition for the material balance

$$\int_0^1 s_{SZ}(X, T) dX = s_f DT + s_{ir}(1 - DT) \tag{B-3}$$

We can calculate the integral on the left hand side of Eq. B-3, taking into account that the saturation in the first zone (for  $X > DT + \epsilon\omega_0$ , Fig. 2) is equal to the initial saturation. Also using Eq. 23 to change the variable of the integral

$$\begin{aligned} & \int_0^{DT + \epsilon\omega_0} s_{SZ}(X, T) dX + s_{ir}(1 - DT - \epsilon\omega_0(T)) \\ &= \epsilon \int_{-DT/\epsilon}^{\omega_0} s(\omega) d\omega + s_{ir}(1 - DT - \epsilon\omega_0(T)) \end{aligned} \tag{B-4}$$

Let us change the integration variable in Eq. B-4 from  $\omega$  to  $s$  using Eq. A-6 and substitute the result into the material balance equation (Eq. B-3):

$$\epsilon \int_{s_{ir}}^{s(-DT/\epsilon)} s \frac{-\psi'(s) ds}{f - D(s - s_{ir})} = s_f DT + s_{ir}\epsilon\omega_0(T) \tag{B-5}$$

Writing Eq. A-10 for  $\omega = (-DT/\epsilon)$  saturations  $s = s(-DT/\epsilon)$  for a given moment  $T$ :

$$\int_{s_{ir}}^{s(-DT/\epsilon)} \frac{\Psi'(s) ds}{f - D(s - s_{ir})} = \frac{-DT}{\epsilon} - \omega_0(T) \tag{B-6}$$

Solving Eqs. B-5 and B-6

$$\epsilon \int_{s_{ir}}^{s(-DT/\epsilon)} (s - s_{ir}) \frac{\psi'(s) ds}{D(s - s_{ir}) - f} = (s_f - s_{ir}) DT \tag{B-7}$$

For oil injection, Eqs. B-1–B-7 can be reproduced as follows:

$$1 - \int_0^1 (s_{BL} + s_{SZ} - s_{sh}) dX = T \tag{B-8}$$

$$1 - \int_0^1 s_{BL}(X, T) dX = T \tag{B-9}$$

$$\int_0^1 s_{SZ}(X, T) dX = s_f DT + (1 - DT) \tag{B-10}$$

$$\begin{aligned} & \int_0^{DT + \epsilon\omega_0} s_{SZ}(X, T) dX + (1 - DT - \epsilon\omega_0(T)) = \epsilon \int_{-DT/\epsilon}^{\omega_0} s(\omega) d\omega \\ & + (1 - DT - \epsilon\omega_0(T)) \end{aligned} \tag{B-11}$$

$$\varepsilon \int_1^{s(-DT/\varepsilon)} s \frac{-\psi'(s) ds}{D(1-s) - (1-f)} = s_f DT + \varepsilon \omega_0(T) \tag{B-12}$$

$$\int_1^{s(-DT/\varepsilon)} \frac{\Psi'(s) ds}{D(1-s) - (1-f)} = \frac{-DT}{\varepsilon} - \omega_0(T) \tag{B-13}$$

$$\varepsilon \int_{s(-DT/\varepsilon)}^1 (1-s) \frac{\psi'(s) ds}{D(1-s) - (1-f)} = (1-s_f) DT \tag{B-14}$$

Equations B-7 and B-14 determine the value  $s(-DT/\varepsilon)$  at each moment,  $T$  for water and oil injections, respectively. The value  $\omega_0(T)$  is calculated from Eq. B-6 or B-13 at each moment,  $T$ . Equations A-10 or A-11 are then used to determine the saturation profile in the stabilized zone.

### Appendix C: Asymptotic End-effect Solution

Let us derive the saturation distribution at the outlet of the core after Barenblatt et al. (1991). Introducing the inner variable (Eq. 27) into Eq. 1:

$$\varepsilon \frac{\partial s}{\partial T} - \frac{\partial f}{\partial \zeta} = \frac{\partial^2 \Psi}{\partial \zeta^2} \tag{C-1}$$

As discussed before in Sect. 2.3 that the end-effect saturation profile does not depend on the type of the fluid injected but the wettability preference of the rock; we shall describe the solution of Eq. C-1 for boundary conditions (Eqs. 10–15) for different wettability preferences. The boundary condition given by Eqs. 10–15 for the inner coordinate after the breakthrough takes the following form, for water-wet rock

$$\zeta = 0: s = s^0 \tag{C-2}$$

and for oil wet rock

$$\zeta = 0: s = s_{ir} \tag{C-3}$$

When  $\varepsilon$  approaches to zero, the solution of Eq. C-1 is the same as the large-scale approximation, i.e. Eqs. 19–22.

$$\zeta \rightarrow \infty: s(\zeta) \rightarrow s_{BL}(1, T) \tag{C-4}$$

Neglecting the  $\varepsilon$ -order-term in Eq. C-1 yields an ordinary differential equation. Let us reduce the order of the ordinary differential equation by taking into account the condition given by Eq. C-4

$$\frac{d\Psi}{d\zeta} = f(s_{BL}(1/T)) - f(s) \tag{C-5}$$

Separating variables in Eq. C-5 and integrating w.r.t.  $s$

$$\zeta = \int_s^{s(\zeta=0)} \frac{\Psi'(s) ds}{-f(s) + f(s_{BL}(1/T))} \tag{C-6}$$

We can write Eq. C-5 for boundary conditions given by Eqs. C-2 and C-3 as,  
 For water-wet system

$$(1 - X)/\varepsilon = \int_s^{s^0} \frac{\Psi'(s) ds}{-f(s) + f(s_{BL}(1/T))} \tag{C-7}$$

For oil wet system

$$(1 - X)/\varepsilon = \int_{s_{ir}}^s \frac{\Psi'(s) ds}{f(s) - f(s_{BL}(1/T))} \tag{C-8}$$

Equations C-7 and C-8 give the end-effect saturation profile for the water- and oil-wet systems, respectively. For a mixed wet system, the end-effect saturation profile is weighted average of saturations derived from Eqs. C-7 and C-8 on the basis of the fraction of water- and oil-wet surfaces in the rock, i.e.

$$s_{EE}(\zeta, mixed\_wet) = s_{EE}(\zeta, water\_wet) \times F_{w\_wet} + s_{EE}(\zeta, oil\_wet) \times (1 - F_{w\_wet}) \tag{C-9}$$

### Appendix D: Pressure Drop Calculations for the Global Asymptotic Solution

The pressure drop in the core can be calculated from

$$\Delta p(T) = \int_0^1 -\frac{\partial P}{\partial X} dX \tag{D-1}$$

Let us express the pressure gradient in the water phase and oil phase from the modified-Darcy’s law (Eqs. 5a and 5b) and substitute it into Eq. D-1

$$\frac{k\Delta p_w(T)}{LU\mu_o} = \frac{1}{\mu_o} \int_0^1 \frac{dX}{\lambda(s)} + \varepsilon \int_0^1 \frac{k_{ro}}{\mu_o} \frac{\partial J(s)}{\partial X} \frac{dX}{\lambda(s)} \tag{D-2}$$

or

$$\frac{k\Delta p_w(T)}{LU\mu_o} = \frac{1}{\mu_o} \int_0^1 \frac{dX}{\lambda(s)} + \varepsilon \int_{s(X=0)}^{s(X=1)} (1 - f(s)) J'(s) ds \tag{D-3}$$

Once the saturation profile is known at any moment  $T$ , Eq. D-3 can be used to calculate pressure drop through the water phase in the core. Similarly for the oil phase:

$$\frac{k\Delta p_o(T)}{LU\mu_o} = \frac{1}{\mu_o} \int_0^1 \frac{dX}{\lambda(s)} - \varepsilon \int_{s(X=0)}^{s(X=1)} f(s) J'(s) ds \tag{D-4}$$

During coreflooding, the pressure drop is measured outside the core where the capillary pressure is zero, which means that the oil and water phase pressures are the same. For this reason, some researchers have suggested that, since the pressure drop in both phases is the same, any of the above equations (Eq. D-3 or D-4) can be used to calculate pressure drop

across the core (Civan and Donaldson 1989). But, if we consider oil injection in a water-wet core, the second integral term in Eq. D-3 becomes infinite (consider the inlet boundary) while Eq. D-4 still gives a finite pressure drop. Physical reason for this phenomenon is that, at the inlet water is a discontinuous phase while oil is continuous. Hence, we can conclude that for oil injection oil is the continuous phase throughout the core and the measured pressure drop can be calculated from Eq. D-4. Similarly, Eq. D-3 should be used for water flooding. Ramakrishnan and Cappiello (1991); Virnovsky et al. (1995) and Hussain et al. (2010) have adapted a similar assumption for the pressure drop calculations.

## References

- Alizadeh, A.H., Keshavarz, A., Haghghi, M.: Flow rate effect on two-phase relative permeability in Iranian carbonate rocks. In: SPE middle east oil and gas show and conference, Bahrain, 11–14 Mar 2007
- Amyx, J., Bass, D., Whiting, R.: Petroleum reservoir engineering: physical properties. McGraw-Hill College, New York (1960)
- Anderson, W.: Wettability literature survey part 5: the effects of wettability on relative permeability. *J. Petroleum Technol.* **39**, 1453–1468 (1987)
- Bacri, J.C., Leygnac, C., Salin, D.: Evidence of capillary hyperdiffusion in two-phase fluid flows. *J. Phys. Lett.* **46**, 467–473 (1985)
- Barenblatt, G., Entov, V., Ryzhik, V.: Theory of fluid flows through natural rocks. Kluwer Academic Publishers, Dordrecht (1991)
- Basbug, B., Karpyn, Z.: Determination of relative permeability and capillary pressure curves using an automated history-matching approach. In: SPE eastern regional/AAPG eastern section joint meeting, Pittsburgh, 11–15 Oct 2008
- Batycky, J., Mccaffery, F., Hodgins, P., Fisher, D.: Interpreting relative permeability and wettability from unsteady-state displacement measurements. *Old SPE J.* **21**, 296–308 (1981)
- Bedrikovetsky, P.: Mathematical theory of oil and gas recovery: with applications to ex-USSR oil and gas fields. Kluwer Academic Publishers, Boston (1993)
- Bedrikovetsky, P., Rodrigues, J., Britto, P.: Analytical model for the waterflood honouring capillary pressure (with applications to laboratory studies). In: SPE Latin America/Caribbean petroleum engineering conference, Port-of-Spain, 23–26 Apr 1996
- Buckley, S., Leverett, M.: Mechanism of fluid displacement in sands. *Trans. AIME.* **146**, 107–116 (1942)
- Burdine, N., Gournay, L., Reichertz, P.: Pore size distribution of petroleum reservoir rocks. *Trans. AIME.* **189**, 195–204 (1950)
- Chardaire-Riviere, C., Chavent, G., Jaffre, J., Liu, J., Bourbiaux, B.: Simultaneous estimation of relative permeabilities and capillary pressure. *SPE Form. Evaluation* **7**, 283–289 (1992)
- Christiansen, R.: Two-phase flow through porous media. Colorado School of Mines, Golden (2001)
- Civan, F., Donaldson, E.: Relative permeability from unsteady-state displacements with capillary pressure included. *SPE Form. Evaluation* **4**, 189–193 (1989)
- Donnez, P.: Essentials of reservoir engineering. Technip Editions, Paris (2007)
- Erdélyi, A.: Asymptotic expansions. Dover Pubns, New York (1956)
- Gel'fand, I.: Some problems in the theory of quasi-linear equations. *Uspekhi Matematicheskikh Nauk* **14**, 87–158 (1959)
- Hamming, R.: Numerical methods for scientists and engineers. Dover Publications, Mineola (1986)
- Honarpour, M., Koederitz, L., Harvey, A.: Relative permeability of petroleum reservoirs. CRC Press, Boca Raton (1986)
- Huang, D., Honarpour, M.: Capillary end effects in coreflood calculations. *J. Petroleum Sci. Eng.* **19**, 103–118 (1998)
- Hussain, F., Cinar, Y., Bedrikovetsky, P.: Comparison of methods for drainage relative permeability estimation from displacement tests. In: SPE IOR Symposium, Tulsa (2010)
- Islam, M., Bentsen, R.: A dynamic method for measuring relative permeability. *JCPT*, Jan–Feb, pp. 39–50 (1986)
- Johnson, E., Bossler, D., Naumann, V.: Calculation of relative permeability from displacement experiments. *Trans. AIME.* **216**, 370–372 (1959)
- Jones, S., Roszelle, W.: Graphical techniques for determining relative permeability from displacement experiments. *J. Petroleum Technol.* **30**, 807–817 (1978)

- Kalbus, J., Christiansen, R.: New data reduction developments for relative permeability determination. In: ATC & Exhibition, Dallas, 22–25 Oct 1995
- Kerig, P., Watson, A.: Relative-permeability estimation from displacement experiments: an error analysis. *SPE Reserv. Eng.* **1**, 175–182 (1986)
- Kevorkian, J., Cole, J., John, F.: *Perturbation methods in applied mathematics*. Springer-Verlag, New York (1981)
- Krause, M., Perrin, J.C., Benson, S.: Recent progress in predicting permeability distributions for history matching core flooding experiments. *Energy Procedia* **4**, 4354–4361 (2011)
- Nayfeh, A.: *Perturbation methods*. Wiley, New York (1973)
- Nordtvedt, J., Urkedal, H., Ebeltoft, E., Kolltveit, K., Petersen, E., Sylte, A., Valestrand, R.: The significance of violated assumptions on core analysis results. In: *International symposium of the society of core analysts*, Golden (1999)
- Odeh, A., Dotson, B.: A method for reducing the rate effect on oil and water relative permeabilities calculated from dynamic displacement data. *J. Petroleum Technol.* **37**, 2051–2058 (1985)
- Perrin, J.C., Benson, S.: An experimental study on the influence of sub-core scale heterogeneities on CO<sub>2</sub> distribution in reservoir rocks. *Transp. Porous Med.* **82**, 93–109 (2010)
- Poulsen, S., Skauge, T., Dyrhol, S., Stenby, E.H., Skauge, A.: Including capillary pressure in simulations of steady state relative permeability experiments. In: *International symposium of the society of core analysts*, Abu Dhabi (2000)
- Purcell, W.: Capillary pressures—their measurement using mercury and the calculation of permeability therefrom. *Trans. Am. Inst. Min. Metall. Pet. Eng.* **186**, 39–48 (1949)
- Qadeer, S.: *Techniques to handle limitations in dynamic relative permeability measurements*. Stanford University, California (2001)
- Qadeer, S., Brigham, W., Castanier, L.: *Techniques to handle limitations in dynamic relative permeability measurements*. National petroleum technology office, Tulsa, Prepared for US Department of Energy Assistant Secretary for Fossil Energy, p. 142 (2002)
- Qadeer, S., Dehghani, K., Ogbe, D., Ostermann, R.: Correcting oil/water relative permeability data for capillary end effect in displacement experiments. In: *SPE California regional meeting*, Long Beach, 23–25 Mar (1988)
- Ramakrishnan, T., Cappiello, A.: A new technique to measure static and dynamic properties of a partially saturated porous medium. *Chem. Eng. Sci.* **46**, 1157–1163 (1991)
- Rapoport, L., Leas, W.: Properties of linear waterfloods. *Trans. AIME.* **198**, 139–148 (1953)
- Richmond, P., Watson, A., Texas, A.: Estimation of multiphase flow functions from displacement experiments. *SPE Reserv. Eng.* **5**, 121–127 (1990)
- Sigmund, P., Mccaffery, F.: An improved unsteady-state procedure for determining the relative-permeability characteristics of heterogeneous porous media. *Soc. Petroleum Eng. J.* **19**, 15–28 (1979)
- Subbey, S., Monfared, H., Christie, M., Sambridge, M.: Quantifying uncertainty in flow functions derived from SCAL data. *Trans. Porous Med.* **65**, 265–286 (2006)
- Tikhonov, A., Arsenin, V., John, F.: *Solutions of ill-posed problems*. Vh Winston, Washington (1977)
- Toth, J., Bodi, T., Szucs, P., Civan, F.: Convenient formulae for determination of relative permeability from unsteady-state fluid displacements in core plugs. *J. Petroleum Sci. Eng.* **36**, 33–44 (2002)
- Tsakiroglou, C., Avraam, D., Payatakes, A.: Simulation of the immiscible displacement in porous media using capillary pressure and relative permeability curves from transient and steady-state experiments. In: *International symposium of the society of core analysts*, Abu Dhabi, UAE (2004)
- Udegbunam, E.: A FORTRAN program for interpretation of relative permeability from unsteady-state displacements with capillary pressure included. *Comput. Geosci.* **17**, 1351–1357 (1991)
- Van Dyke, M.: *Perturbation methods in fluid mechanics/Annotated edition*. NASA STI/Recon Tech. Report A. **75**, 46926 (1975)
- Virnovsky, G., Skjaeveland, S., Surdal, J., Ingsøy, P.: Steady-state relative permeability measurements corrected for capillary effects. In: *SPE annual technical conference and exhibition*, Dallas, 22–25 Oct 1995
- Welge, H.: A simplified method for computing oil recovery by gas or water drive. *Trans. Am. Inst. Min. Metall. Petrol. Eng.* **195**, 91–98 (1952)